Science Translational Medicine
AAAS

www.sciencetranslationalmedicine.org/cgi/content/full/8/340/340ra73/DC1

Supplementary Materials for

Dormant breast cancer micrometastases reside in specific bone marrow niches that regulate their transit to and from bone

Trevor T. Price, Monika L. Burness, Ayelet Sivan, Matthew J. Warner, Renee Cheng, Clara H. Lee, Lindsey Olivere, Karrie Comatas, John Magnani, H. Kim Lyerly, Qing Cheng, Chad M. McCall, Dorothy A. Sipkins*

*Corresponding author. Email: dorothy.sipkins@dm.duke.edu

Published 25 May 2016, *Sci. Transl. Med.* **8**, 340ra73 (2016)
DOI: 10.1126/scitranslmed.aad4059

This PDF file includes:

Other Supplementary Material for this manuscript includes the following:
(available at www.sciencetranslationalmedicine.org/cgi/content/full/8/340/340ra73/DC1)

Video S1 (.mov format). Circulating BCCs crawling along vascular wall (merge).
Video S2 (.mov format). Circulating BCCs crawling along vascular wall (DiD channel only).
Video S3 (.mov format). Circulating BCCs before AMD3100 treatment (merge).
Video S4 (.mov format). Circulating BCCs before AMD3100 treatment (DiD channel only).
Video S5 (.mov format). Circulating BCCs after AMD3100 treatment (merge).
Video S6 (.mov format). Circulating BCCs after AMD3100 treatment (DiD channel only).

Supplementary Materials and Methods:

Quantitative RT-PCR (qRT-PCR)

Total RNA was extracted from BCC lines and primary breast cancer cells using Qiazol and miRNeasy RNA extraction kits (Qiagen). cDNA synthesis was completed using the Superscript VILO reverse transcriptase (Thermo Fisher Scientific), and qRT-PCR quantification of *GLG1, LGALS3BP, MUC1, SELPLG, LAMP1, B4GALT6,* and *CXCR4* was performed with Taqman gene expression assays (Thermo Fisher Scientific). Relative mRNA expression was calculated using the $\Delta\,\Delta\mathrm{CT}\ \mathrm{method}$ after normalization to *MRPL13*.

Western blotting

Protein was extracted from BCC lines using RIPA buffer: 150 mM NaCl; 10 mM Tris HCl pH 7.2; 0.1% SDS; 0.1% Triton X-100; 1% sodium deoxycholate; 5 mM EDTA; 1% protease (P8340 - Sigma). Equal amounts of total protein were resolved on Mini-PROTEAN TGX gels and transferred to Immun-Blot PVDF membrane with a Mini Trans-Blot cell (BioRad). Antibodies against LAMP1 (#9091, D2D11) and MUC1 (#14161, D908K) were purchased from Cell Signaling Technology. Antibodies for GLG1 (AF7879-SP) were purchased from R&D Systems, and LGALS3BP (ab191186) and β-actin (ab6276) from Abcam. Reactivity was detected with HRP-conjugated secondary antibodies and quantified by ECL (Thermo Fisher Scientific). Densitometry was performed using ImageJ software.

Immunoprecipitation

All cell lines were lysed with ice-cold lysis buffer (1% Triton X-100, 150 mM NaCl, 50 mM Tris-HCl pH 7.4, 1 mM EDTA, 1 mM EGTA, protease inhibitor cocktail +/- 500 μM Siastatin B). Lysates were centrifuged at 12,000 g for 5 minutes, and supernatants were cleared with Protein G Dynabeads (ThermoFisher Scientific) for 1 hour at 4^{o}C. MUC1 antibody (Cell Signaling) was then added to each of the collected lysates at the manufacturer's recommended dilution and incubated at 4^{o}C overnight under constant rotation. Lysates were then incubated with Protein G Dynabeads for 2 hours at 4^{o}C, before magnetically sequestering the Dynabeads from the lysates, followed by repeated washes with 1% Triton X-100 lysis buffer containing 1% BSA. Dynabeads were then washed with 1% Triton X-100 lysis buffer and incubated for 5 minutes in Laemmli

sample buffer at 95°C. Immunoprecipitates were subjected to SDS-PAGE and MUC1 immunoblots performed as for those completed with whole cell lysates. Recombinant E-selectin-Fc (R&D Systems) immunoblots were performed after blocking PVDF membranes for 1 hour in 5% BSA-TBS/T, 10 mM HEPES, and 5 mM $CaCl_2$ blocking buffer. E-selectin-Fc was incubated with membranes at 1 μ g/ml overnight at 4°C and detected with goat anti-human IgG HRP secondary antibody (Southern Biotech) by chemiluminescence.

Flow Cytometry

CD44 and E-selectin ligand expression in BCC cell lines was determined by flow cytometry. Sub-confluent cell cultures were trypsinized and counted. For extracellular staining, 1 x 10^6 cells were washed in PBS and resuspended in 100 µl wash buffer (automacs + 3% BSA). Cells were incubated with Live / Dead near I.R stain (Invitrogen) for 20 min on ice. Cells were washed and subsequently incubated with anti-CD44-APC (clone G44-26) or Isotype-APC (clone 27-35) for 30 min on Ice. Cells were spun at 500 g and resuspended in 300 µl 1% PFA in PBS. E-selectin ligand expression analysis was performed using a recombinant human E-selectin / human-Fc chimera protein (E-sel-Fc) (# 724-ES, R&D Systems). Adherent BCCs were dissociated from culture flasks using an enzyme-free dissociation buffer in Hanks Balanced Salt Solution (HBSS) (Gibco). Incubations were performed in a E-sel-Fc chimera buffer of HBSS supplemented with 5% FBS, 5 mM HEPES, and 2 mM $Cacl_2$. Cells were incubated with 10 µg/ml E-sel-Fc on ice, followed by a biotinylated anti-human IgG (#6140-08, Southern Biotech) and streptavidin-PE (BD) conjugate. Flow cytometry acquisition was performed with a FACSCANTO II flow cytometer (BD Bioscience) and analyzed with Flowjo (Tree Star Inc.) software.

CXCR4 siRNA knockdown

CXCR4 siRNA knockdown was performed with pLKO.1, PuroCXCR4 siRNA (#plasmid 12272, Addgene), and pLKO.1 puroGFP siNA control (#12273, Addgene) plasmids. Plasmid transfection was performed with the Lenti-X 293T transfection system, and MDA-MB-231 cells were transduced with harvested lentivirus. Validation of the siRNA knockdown was obtained by qPCR and flow cytometry analysis.

Immunofluorescence

BCC cell lines were seeded into 12-well plates with each well containing an 18 mm sterile coverslip and cultured for 24 hours in appropriate medium. MCF-7 stem and non-stem cells were obtained by flow sorting, as described in the materials and methods section. Cells were washed in PBS and fixed in 3.7% formaldehyde in PBS at 37ºC for 15 min. Fixed cells were stored at 4ºC before staining. For E-sel-Fc staining, coverslips were blocked in Hanks balanced salt solution (HBSS) + 5% BSA for 1 hour at room temperature. Appropriate samples were incubated with 15 µg/ml recombinant human E-selectin-Fc chimera protein (#724-ES, R&D Systems) in HBSS, supplemented with 5 mM HEPES and 5 mM $Cacl_2$, and incubated overnight at 4ºC. Cells were washed in incubation buffer + 0.05% Tween (x3, 5 min). Appropriate samples were incubated with 15 µg/ml FITC conjugated anti-human IgG-Fc (#02-10-20, KPL, Inc.) in incubation buffer. Samples were incubated for 1 hour, covered. For MUC1 staining, coverslips were blocked with PBS + 2.5% BSA and incubated with anti-MUC1 (D908K, Cell SIgnaling) overnight at 4ºC in PBS + 1% BSA. Samples were subsequently washed in PBS (x3, 5 min) and incubated with anti-rabbit IgG-AF-647 (#4414, Cell Signaling) for 1 hour at room temperature. Stained cover slips were mounted to slides with prolong gold AntiFade reagent (Cell Signaling) and imaged with a Leica SP5 confocal microscope with 20x/0.40 NA objective lens and DIC optics.

Supplementary Figures:

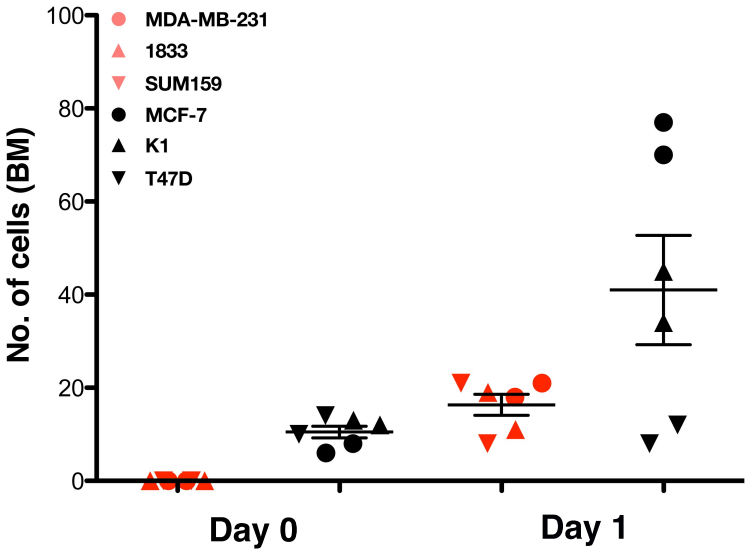

Fig. S1. Bone homing capacity of ER$^+$ and ER$^-$ BCC lines. A panel of ER$^+$ (MCF-7; K1; T47D) and ER- (MDA-MB-231; 1833; SUM159) cell lines were investigated for bone homing capacity. Cells were labeled with lipophilic fluorescent membrane dyes and engrafted into female SCID mice (0.1 x 10^6 cells, I.C. injection). The number of cells homing at Day 0 (2 hours) and Day 1 (20 hours) was quantified via intravital confocal microcopy of the calvarial BM (mean +/- SEM).

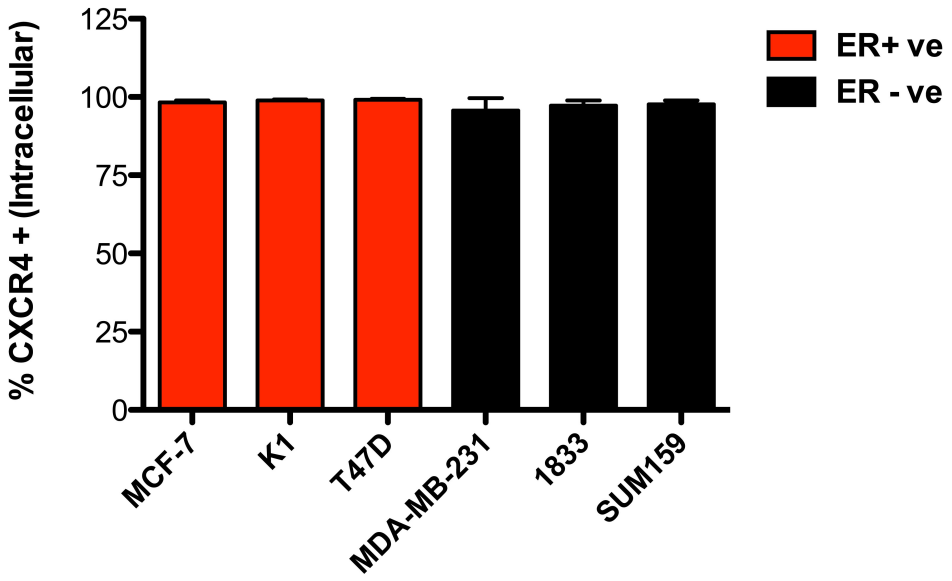

Fig. S2. Intracellular CXCR4 stores expressed in ER$^+$ and ER$^-$ cell lines. Flow cytometric analysis of intracellular CXCR4 expression within ER$^+$ and ER$^-$ BCCs (%CXCR4+ population, *n*=3, mean +/- SEM).

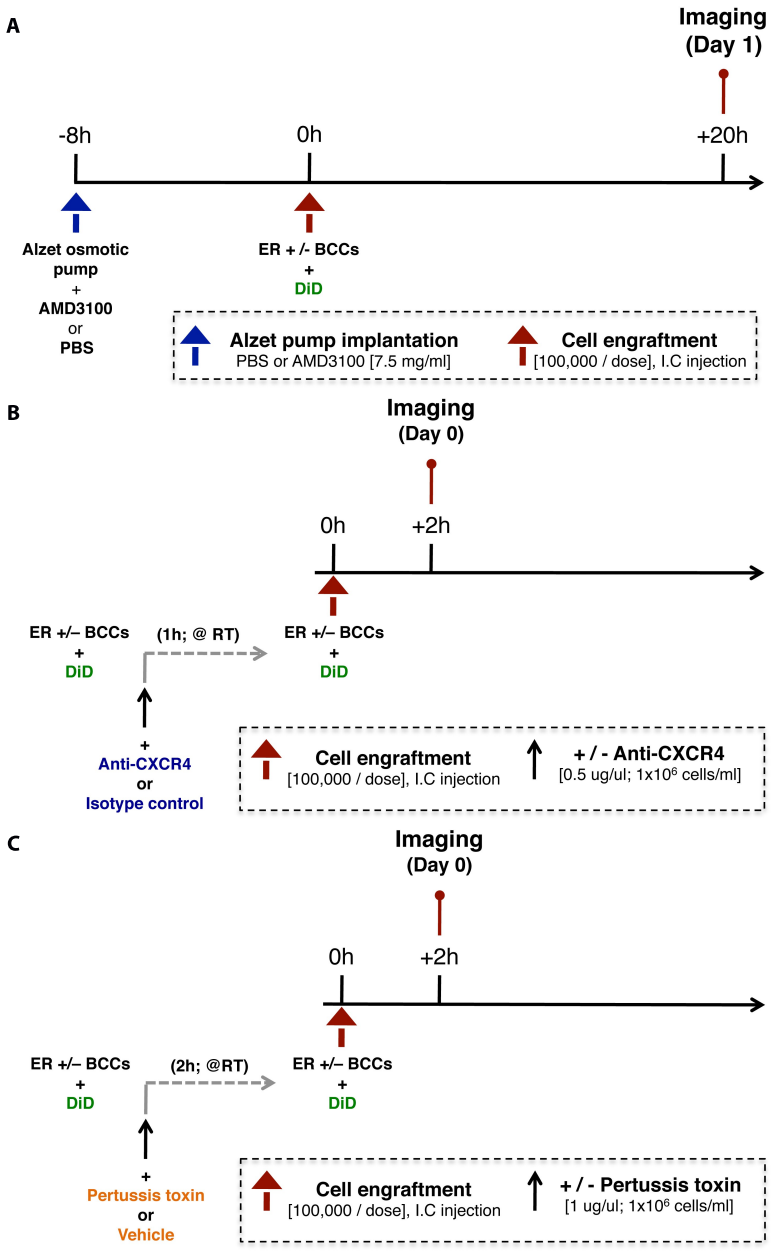

Fig. S3. Schematic for CXCR4-mediated homing inhibition experiments. (**A**) BCC BM homing experiment +/- AMD3100 CXCR4 blockade. (**B**) BCC homing experiment +/- anti-CXCR4 neutralizing antibodies. (**C**) Homing experiment comparing BCCs pretreated with pertussis toxin vs. PBS control.

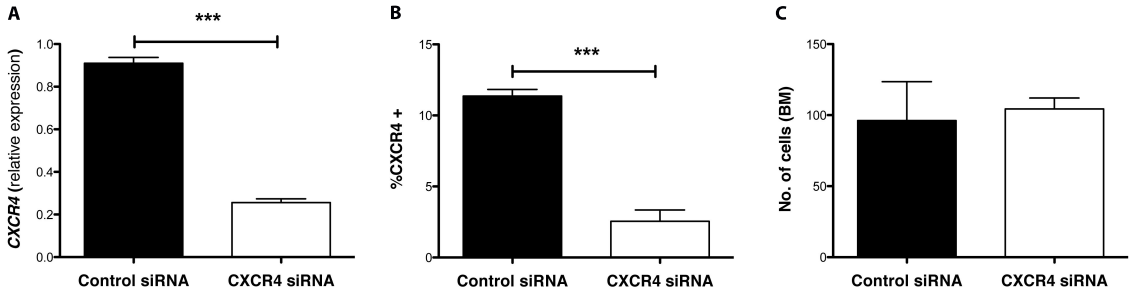

Fig. S4. Effect of CXCR4 siRNA knockdown on BCC BM homing. (**A**) qPCR analysis of *CXCR4* mRNA expression in MDA-MB-231 siRNA control and CXCR4 siRNA knockdown cells (***P*<0.0001, two-tailed unpaired T-test, *n*=3, mean +/- SEM). (**B**) Flow cytometric analysis of CXCR4 cell surface expression on MDA-MB-231 control and CXCR4 knockdown cells (%CXCR4+ populations, ****P*=0.0007, two-tailed unpaired T-test, *n*=3, mean +/- SEM). (**C**) Day 1 (+20 hours after engraftment, 0.1 x 10^6 cells, I.C. injection) homing analysis of DiI stained MDA-MB-231 control and CXCR4 knockdown cells (no. of cells homing to the calvarial BM, *n*=5, mean +/- SEM).

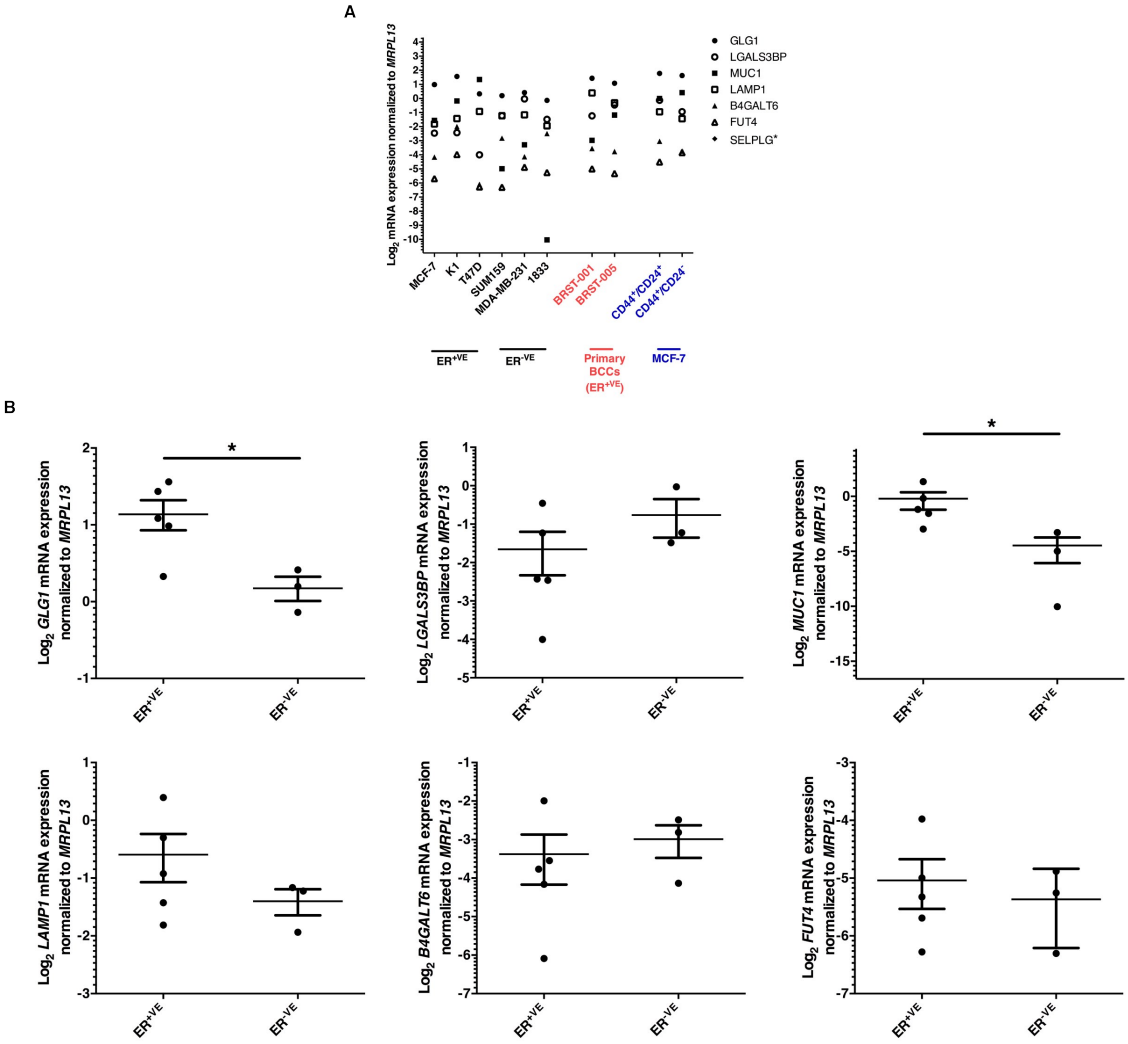

Fig. S5. E-selectin ligand and synthetic enzyme mRNA transcript expression in ER$^+$ and ER$^-$ BCC lines and primary BCCs. (**A**) Scatter plot illustrating mRNA expression of candidate E-selectin ligands and glycosyltransferases in BCCs, primary (ER+) breast cancer cells, and MCF-7 stem ($CD44^+CD24^{-/low}$) and non-stem ($CD44^+CD24^{+/High}$) FACS-isolated cells. * denotes no transcript expression detected for SELPLG in tested samples. (**B**) Log_2 mRNA expression for *GLG1* (ER+: 2.20±0.30; ER-: 1.13±0.12, p = 0.03), *LGALS3BP* (ER+ 0.32-±0.12; ER- 0.59±0.20), *MUC1* (ER+ 0.87±0.44; ER- 0.05±0.03, p = 0.03), *LAMP1* (ER+ 0.66-±0.19; ER- 0.38±0.06), *B4GALT6* (ER+ 0.10-±0.04; ER- 0.13±0.04), and *FUT4* (ER+ 0.03-±0.01; ER- 0.02±0.01). BCCs and primary breast cancer cells were clustered according to their ER expression profile, and statistical analyses were completed using two-tailed unpaired

Student's T-test. Data are presented as values ± SEM, and *P* values are provided above (* = $p < 0.05$).

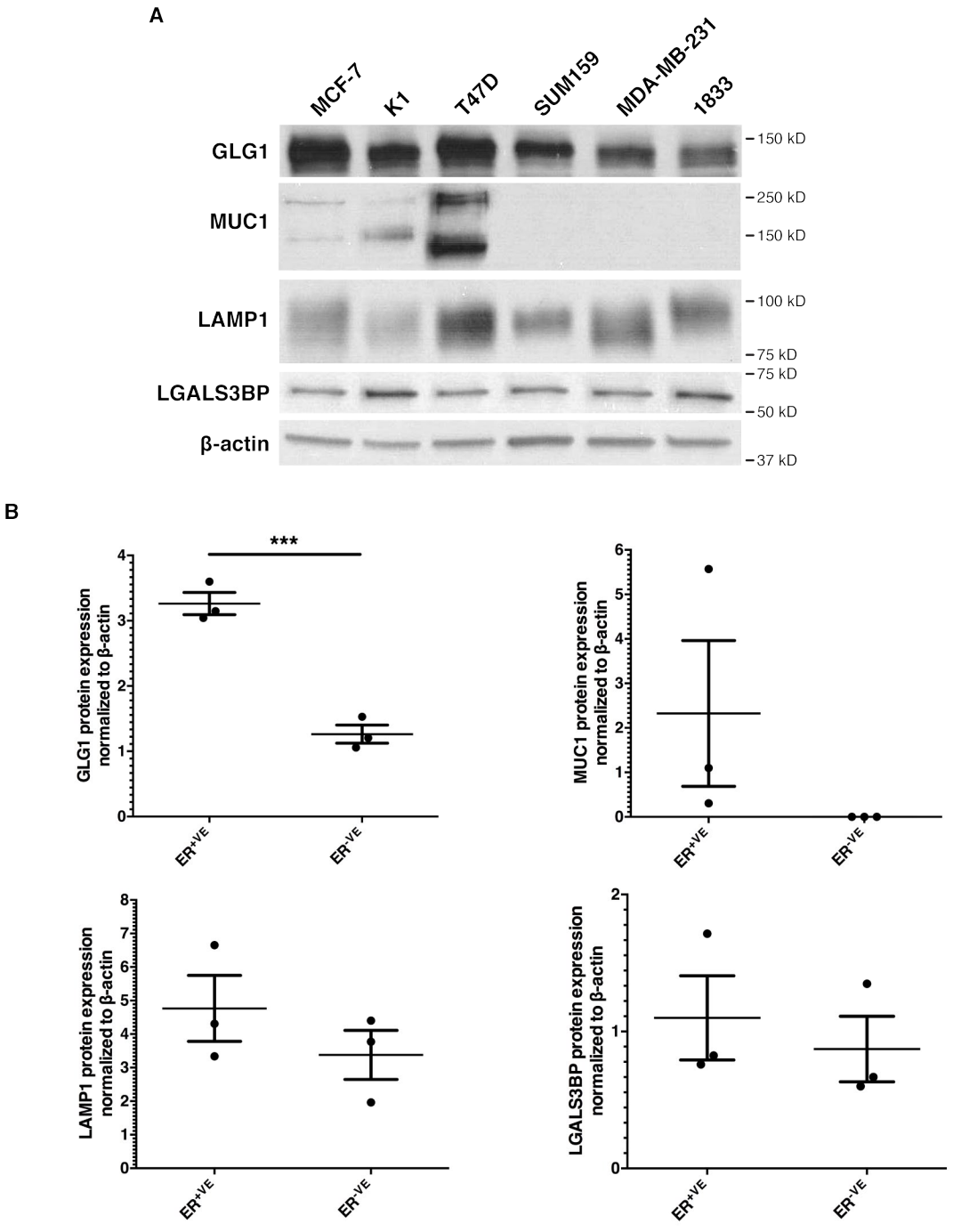

Fig. S6. E-selectin ligand protein expression in ER$^+$ and ER$^-$ BCC lines. (**A**) Immunoblots for GLG1, MUC1, LAMP1, and LGALS3BP in breast cancer cell lines under steady-state growth conditions. (**B**) Densitometry data for GLG1 (ER+: 3.26±0.17; ER-: 1.26±0.14, p = 0.0008), MUC1 (ER+ 2.32-±1.63; ER- no detectable expression),

LAMP1 (ER+ 4.76-±0.98; ER- 3.38±0.73), and LGALS3BP (ER+ 1.10-±0.30; ER- 0.87±0.24). BCCs were clustered according to their ER expression profile, and statistical analyses were completed with two-tailed unpaired student's T-test. Data are presented as values ± SEM, and *P* values are provided above (*** = $p < 0.001$).

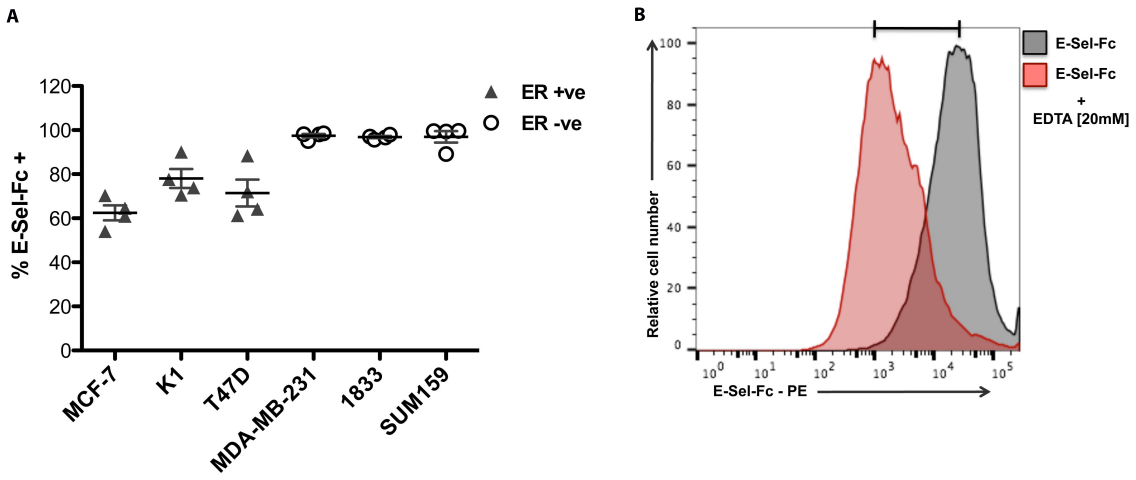

Fig. S7. Flow cytometric analysis of E-selectin ligand expression on BCC lines. (**A**) A panel of ER+ (▲ MCF-7; K1; T47D) and ER- (○ MDA-MB-231; 1833; SUM159) BCC lines was analyzed for E-selectin binding via flow cytometry. The presence of functional E-selectin ligands on BCCs was determined using an E-selectin-Fc chimera protein (R&D Systems) and a biotinylated anti-human Fc and streptavidin-PE detection system (n=3; mean +/- SEM). (**B**) Representative histogram plot of EDTA inhibition of calcium-dependent E-selectin-Fc binding to E-selectin ligands on SUM159 cells.

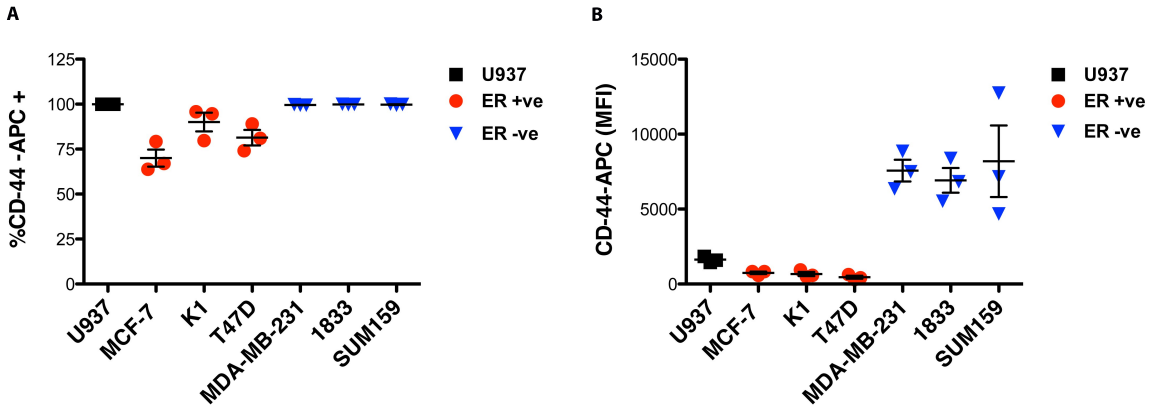

Fig. S8. CD44 cell surface expression on ER$^+$ and ER$^-$ BCC lines. Percentage of CD44+ cells (**A**) and mean fluorescence intensity (MFI) (**B**) in a panel of ER+ and ER- BCCs was analyzed. U937 cells (Human histiocytic lymphoma cell line) were used as a positive control (*n*=3, mean +/- SEM).

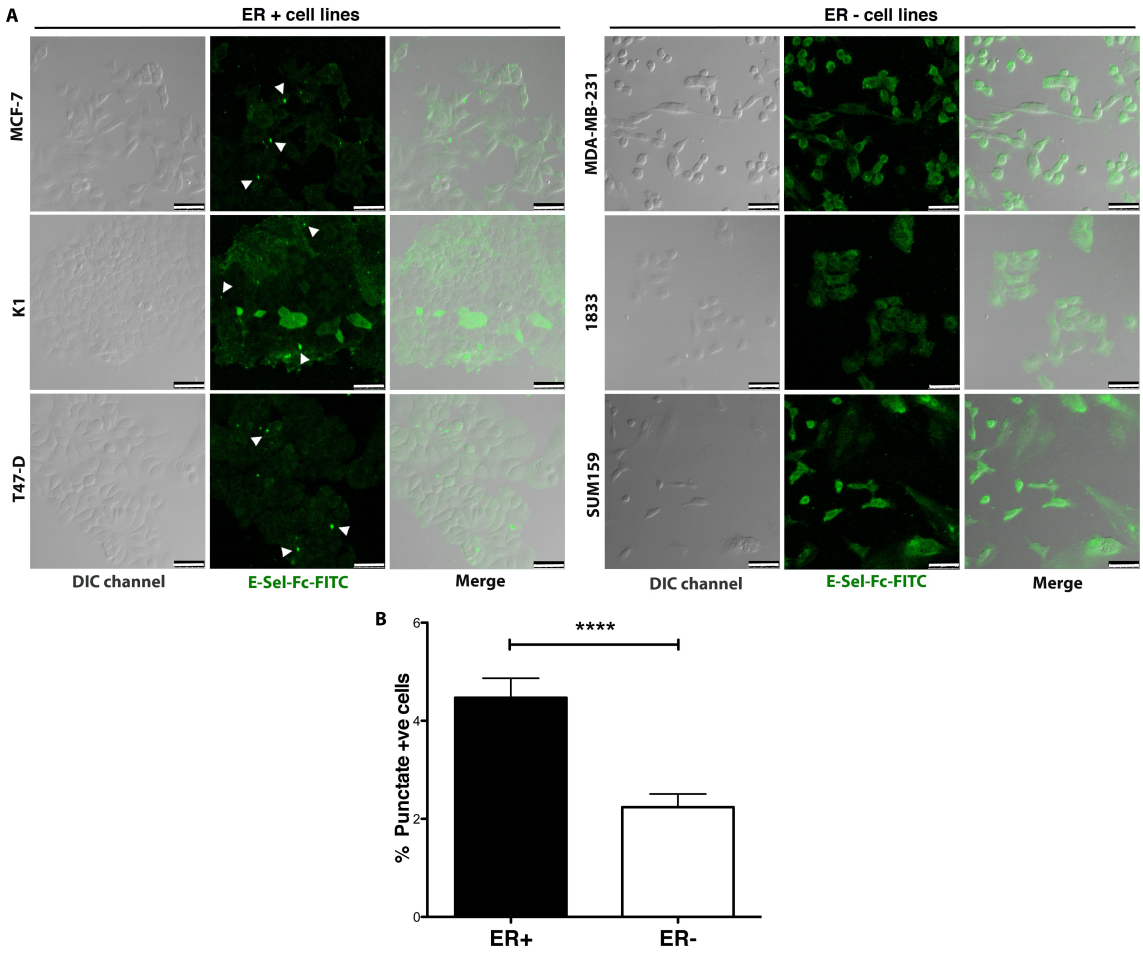

Fig. S9. Immunofluorescence analysis of E-selectin ligand expression on BCC lines. (**A**) Representative images of extracellular E-selectin-Fc binding to ER+ and ER- BCC lines. White arrows indicate punctate areas of E-selectin-Fc binding, suggesting localized clusters of E-selectin ligand expression (representative images of n=3 experiments; scale bars = 50 μm). The presentation of E-selectin ligands in a clustered form may be important in facilitating high avidity ligand-E-selectin binding and downstream signaling events *(48)*. (**B**) Graph of the percentage frequency of punctate positive cells in ER+ vs. ER- cell lines (****P<0.0001, n=50 frames analyzed from three independent experiments, mean +/- SEM).

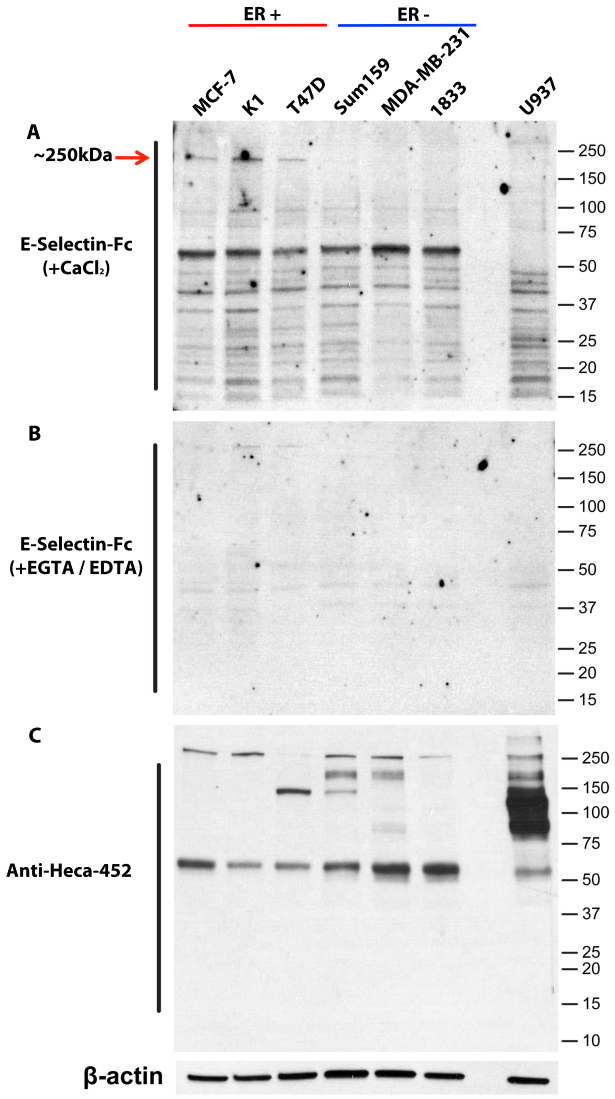

Fig. S10. Western blot analysis of E-selectin ligand expression profiles in BCC lines. The repertoire of functional E-selectin ligands expressed by a panel of ER+ and ER- BCCs was identified by Western blot analysis of whole cell lysates using E-selectin-Fc fusion protein. Entire banding patterns are presented. (**A**) Membrane probed with E-selectin-Fc chimera protein in the presence of Ca2+, required for E-selectin binding. An approximately 250 kDa band is identified in ER+ BCC lines (arrow). (**B**) Calcium-dependent E-selectin ligand-E-selectin-Fc binding was blocked in the presence of EGTA and EDTA Ca2+ chelators. (**C**) Membrane probed with anti-Heca-452 antibody, which recognizes sialyl Lewis^x carbohydrate moieties. Each image is a representative example

of n=3 experiments. Beta-actin loading control is presented. U937 cell lysate used as a positive control for E-selectin ligand expression.

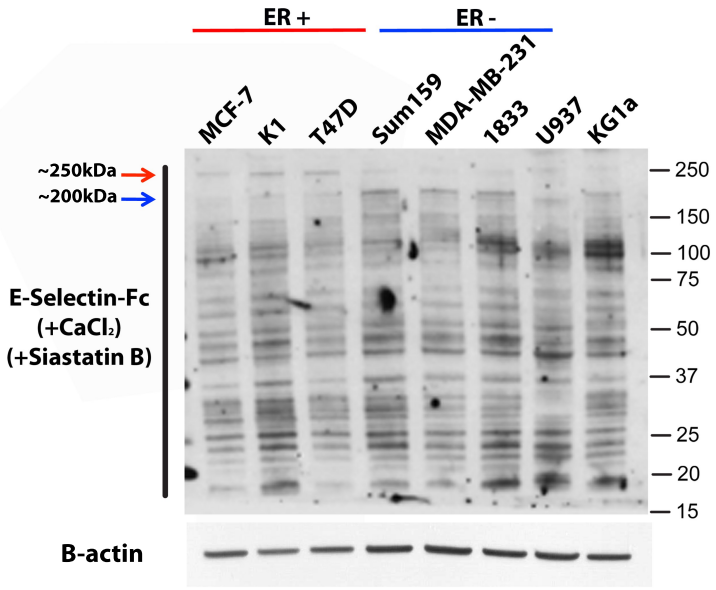

Fig. S11. Western blot analysis of E-selectin ligand expression profiles in BCC lines, with protection of sialic acid residues. E-selectin-Fc chimera protein Western blot analysis was performed, as in Fig. S10, with the addition of the sialidase inhibitor, Siastatin B, to BCC whole cell lysates. An approximately 250 kDa E-selectin ligand is expressed in higher amounts in ER+ vs. ER- BCCs (red arrow), and an approximately 200 kDa ligand is expressed preferentially in ER- cells (blue arrow). . Beta-actin loading control is presented.

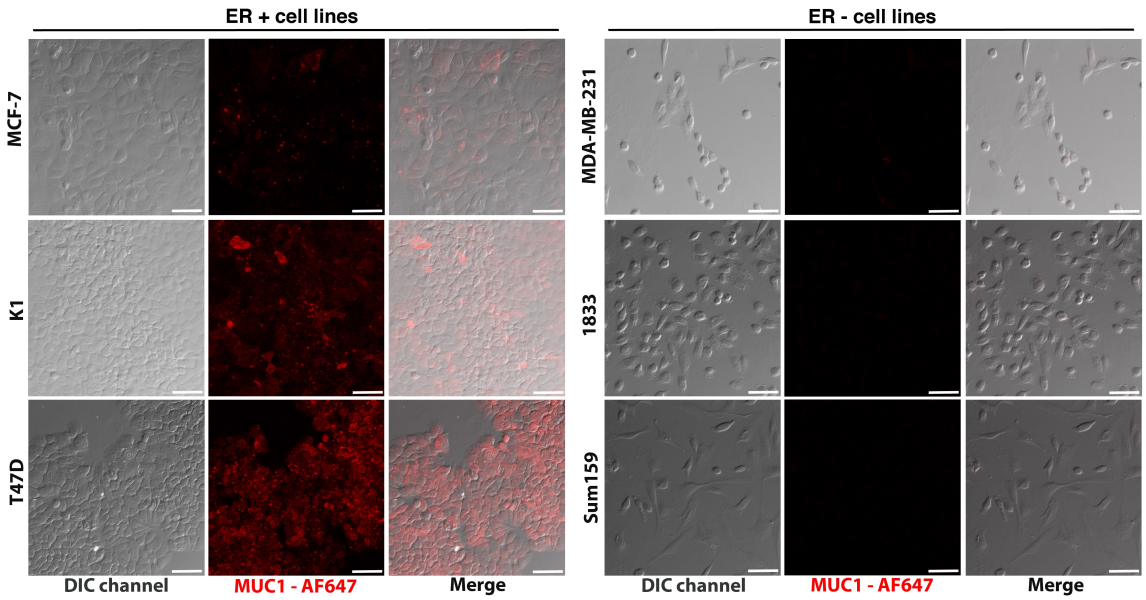

Fig. S12. Immunofluorescence analysis of MUC1 expression on ER$^+$ and ER$^-$ BCCs. Immunofluorescence staining of the panel of ER$^+$ and ER$^-$ BCC lines shows higher expression of extracellular MUC1 by ER$^+$ compared to ER$^-$ BCCs. (representative images of n=3 experiments; scale bars = 50 μm).

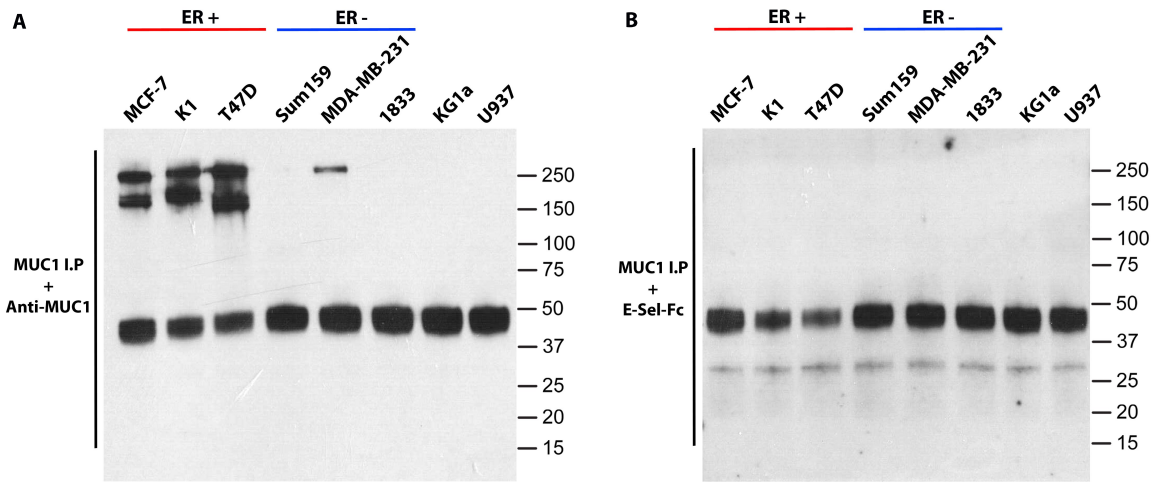

Fig. S13. Immunoprecipitation and functional analysis of the E-selectin binding capacity of MUC1 in BCC lines. Immunoprecipitation (I.P.) of MUC1 was performed in a panel of ER+ and ER- BCCs using an antibody that recognizes the N-terminus of MUC1. (**A**) Anti-MUC1 Western blot analysis was performed as a positive control for successful MUC1 I.P. (**B**) E-selectin-Fc chimera protein was used to probe Western blots of MUC1 I.P. lysates for functional E-selectin ligands, but did not demonstrate binding in this assay. The approximate 45 kDa band observed in all lanes is suspected to be non-specific to MUC1 or E-selectin-Fc probes and is likely a remnant of antibodies used for the MUC1 pull down. Each image is a representative example of n=3 experiments.

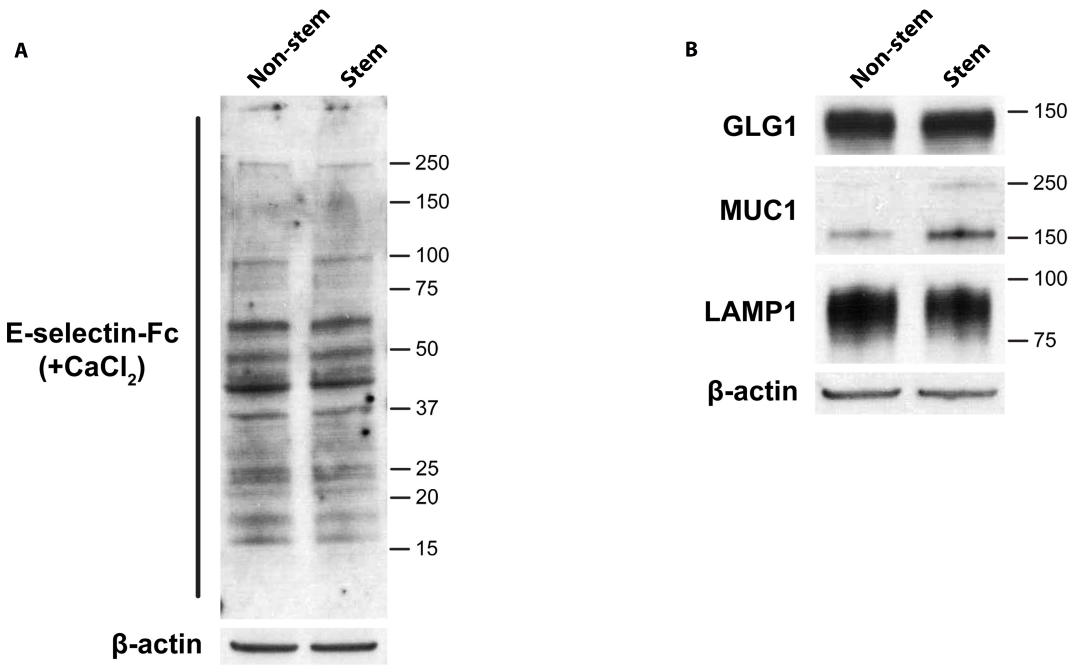

Fig. S14. Western blot analysis of E-selectin ligand expression profiles on MCF-7 stem and nonstem cell populations. MCF-7 stem and nonstem cell populations were isolated by flow sorting, and whole lysates were generated for Western blot analysis. (**A**) Membrane was probed with E-selectin-Fc chimera protein. The entire E-selectin ligand banding profile is presented. (**B**) Membranes were also analyzed for the protein expression of several putative E-selectin ligands (GLG1; MUC1; LAMP1). Beta-actin loading control is presented for both blots.

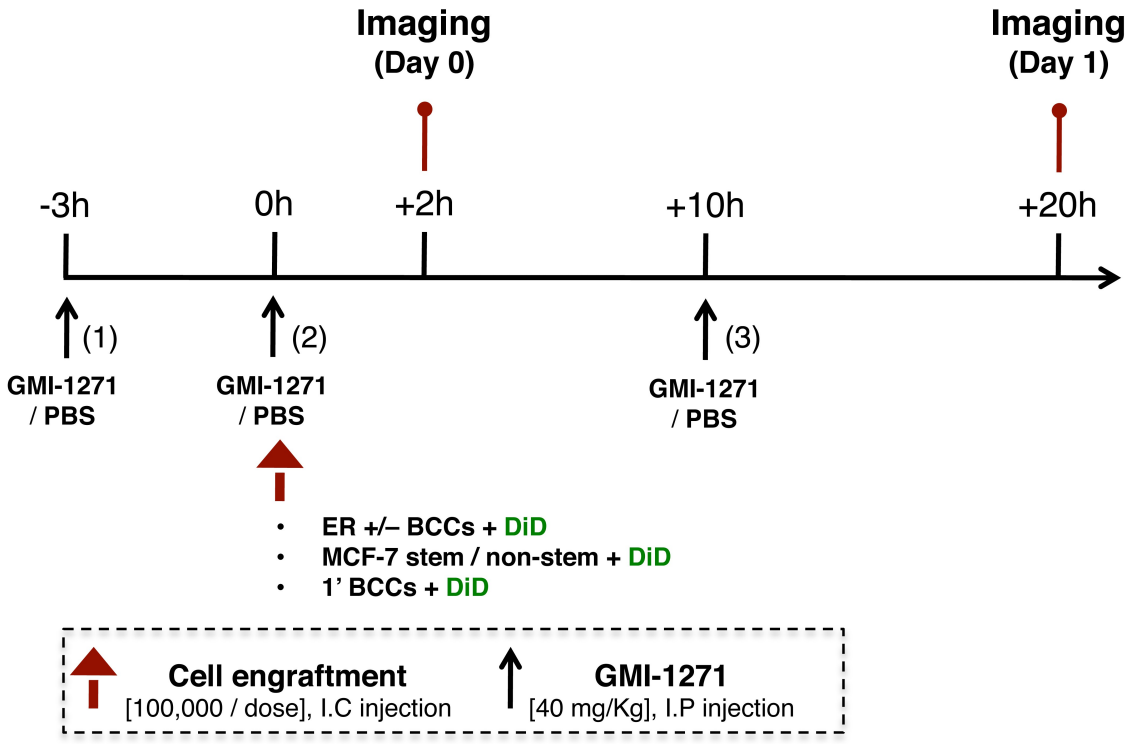

Fig. S15. Schematic for E-selectin-mediated homing inhibition experiments. Dosing strategy for GMI-1271 E-selectin blockade in day 0 (2 hours) and day 1 (20 hours) homing experiments.

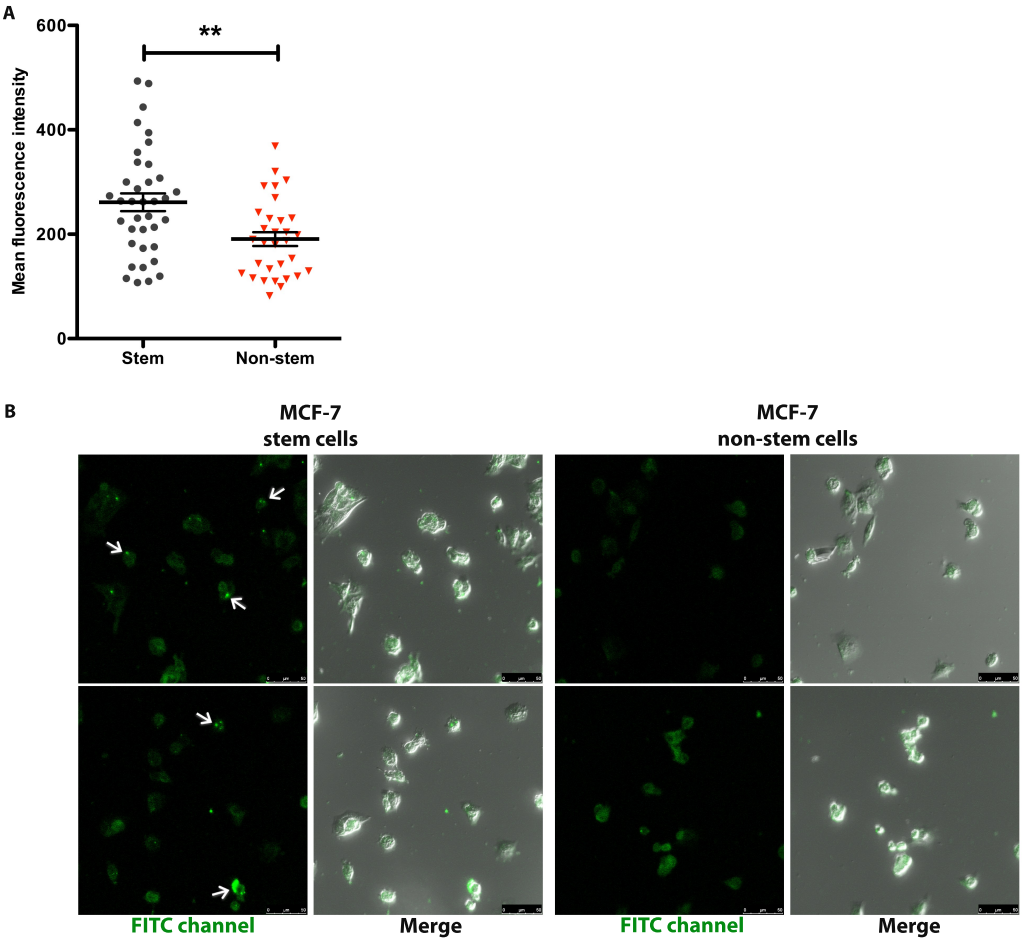

Fig. S16. Immunofluorescence analysis of E-selectin ligand expression on MCF-7 stem and nonstem cell populations. MCF-7 stem ($CD44^{+}/CD24^{-/low}$) and nonstem ($CD44^{+}/CD24^{+/High}$) cells were isolated, and immunofluorescence analysis was performed. MCF-7 stem cells display higher mean fluorescence intensity per cell (**A**, $^{**}P$=0.0023, two-tailed unpaired T-test, mean +/- SEM) and areas of high, localized signal intensity (arrows) (**B**, representative images; scale bars = 50 μm).

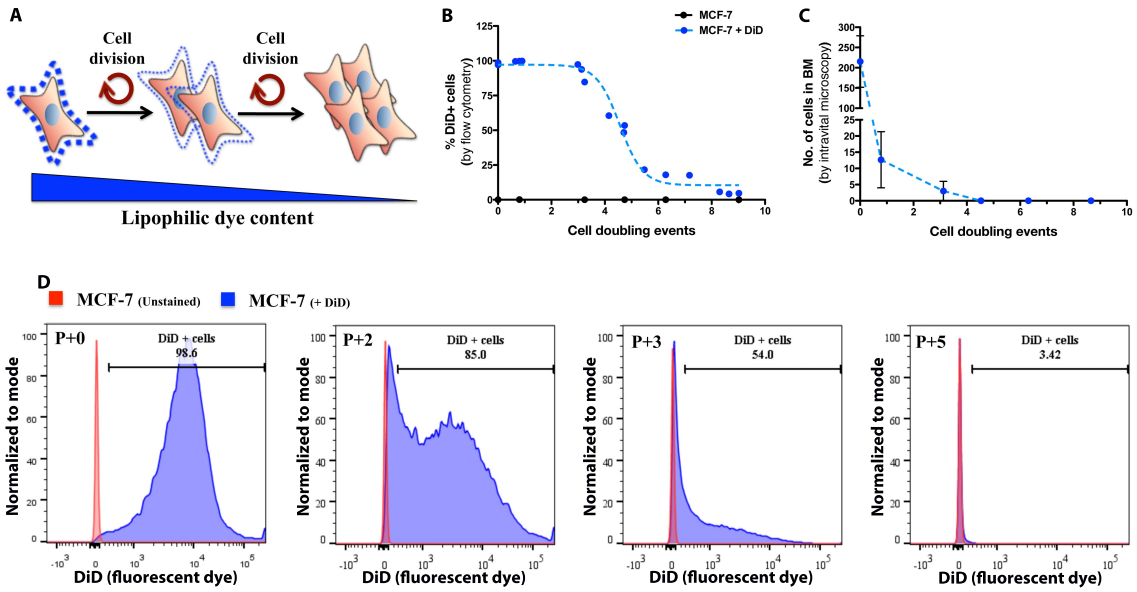

Fig. S17. Fluorescent lipophilic membrane dye depletion after successive cell doubling events. (**A**) Diagram illustrating the dilution and ultimate depletion of fluorescent lipophilic membrane dyes (DiR, DiD, DiI) among daughter cells after successive proliferation events. (**B**) MCF-7 cells were labeled with DiD or PBS control and cultured in vitro. At each passage (P), the number of cell doubling events was determined, and cell fluorescence intensity was analyzed by flow cytometry. The percentage of DiD fluorescent cells vs. doubling time were plotted and regression analysis performed (*n*=3, EC50 [50% dye depletion] = 4.561 cell doubling events; mean +/- SEM). (**C**) DiD-labeled MCF-7 cells cultured in vitro were engrafted into SCID mice at periodic doubling times after staining (doubling events – 0, 0.78, 3.1, 4.5, 6.3, 8.6). The calvarial BM was imaged 20 hours after engraftment, and the number of cells detected was graphed vs. doubling time (*n*=3; mean +/- SEM). (**D**) Representative flow cytometry plots of PBS- (unstained) or DiD-labeled MCF-7 cells at various passage numbers after staining (P+0 = 0 cell doubling events; P+2 = 3.1; P+3 = 4.5; P+5 = 8.6).

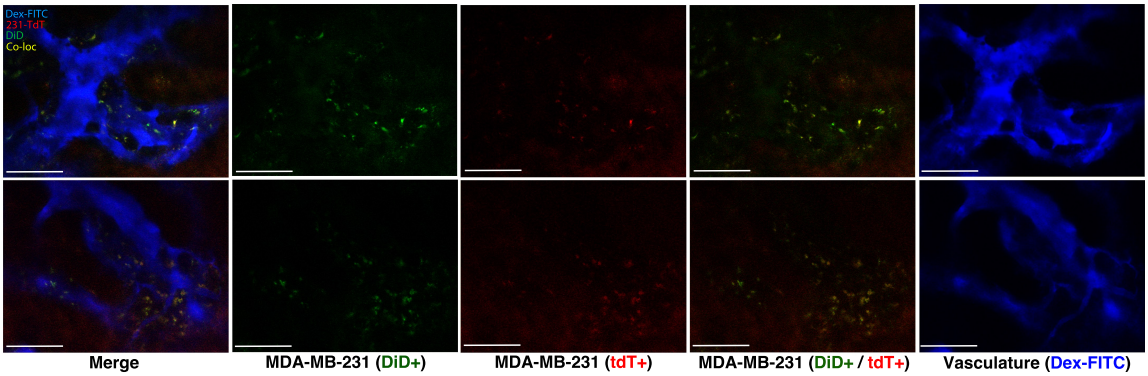

Fig. S18. Spontaneous metastasis of orthotopically engrafted MDA-MB-231 (DiD^+tdT^+) BCCs to the calvarial BM. Single channel images for Fig. 3D (green = DiD, red = tdT, blue = dextran-FITC/vasculature; scale bars = 100 μm).

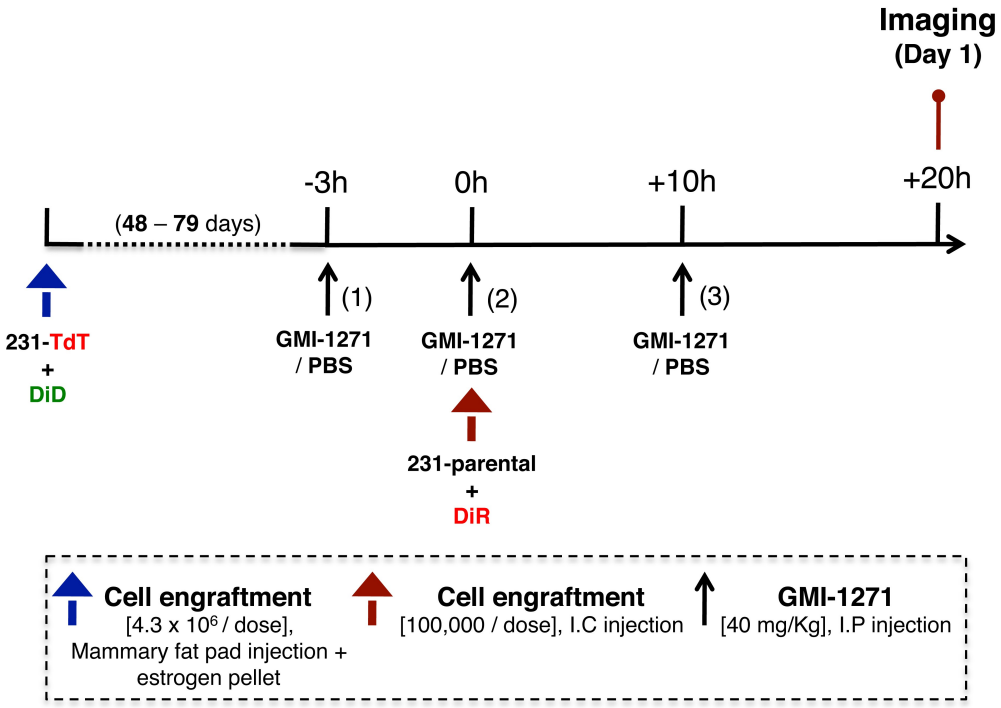

Fig. S19. Schematic for orthotopic engraftment and E-selectin-mediated homing inhibition experiments. Establishment of orthotopic disease in mammary fat pad and dosing strategy for GMI-1271 homing inhibition experiment.

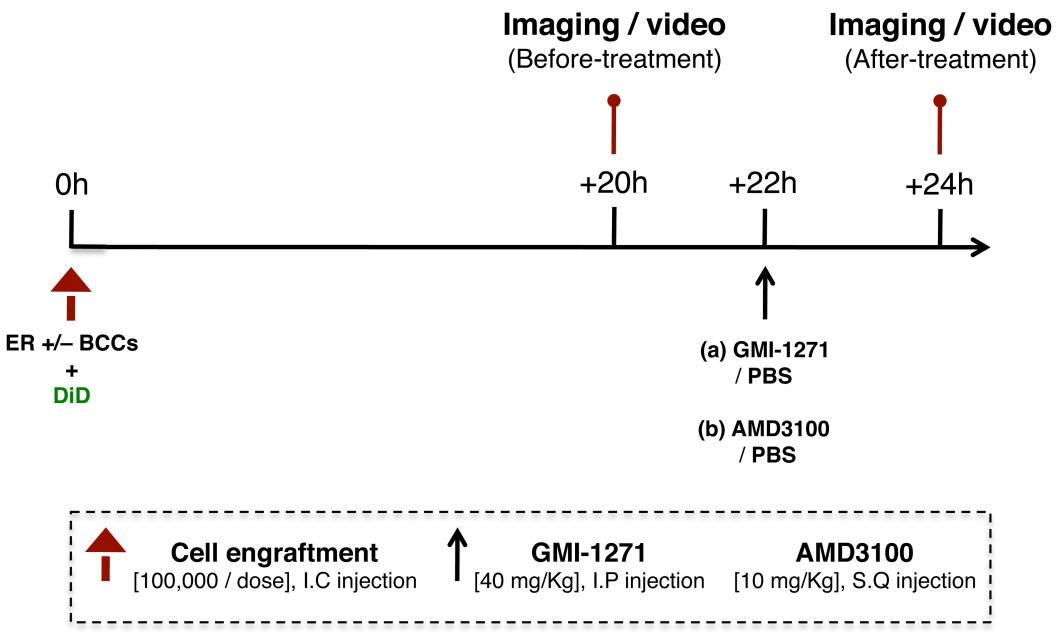

Fig. S20. Schematic for GMI-1271 and AMD3100 mobilization experiments. Day 1 (20 hours) mobilization experiment, +/- AMD3100 or +/- GMI-1271.

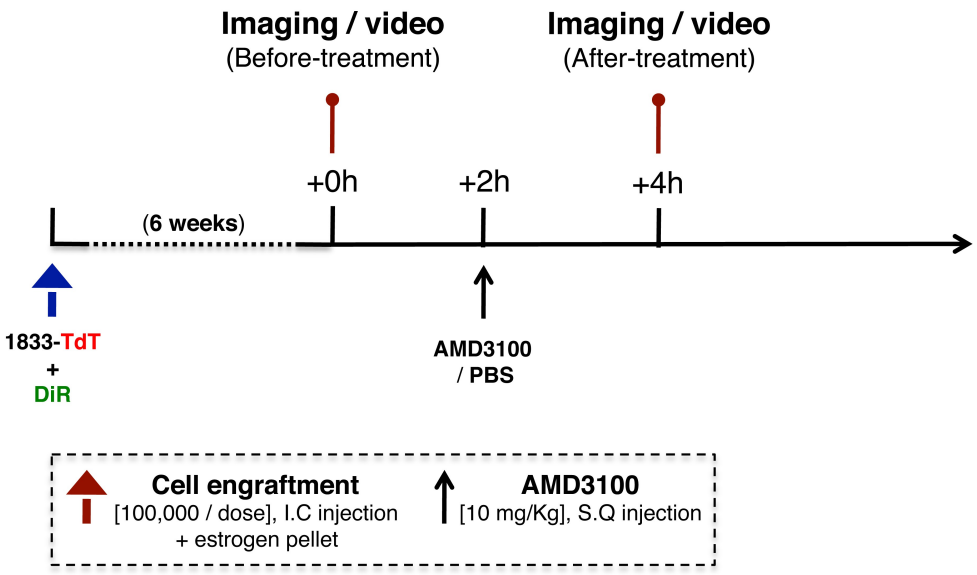

Fig. S21. Schematic for AMD3100 mobilization experiments in mice with established disease. AMD3100 mobilization experiment of established disease, 6 weeks after engraftment.

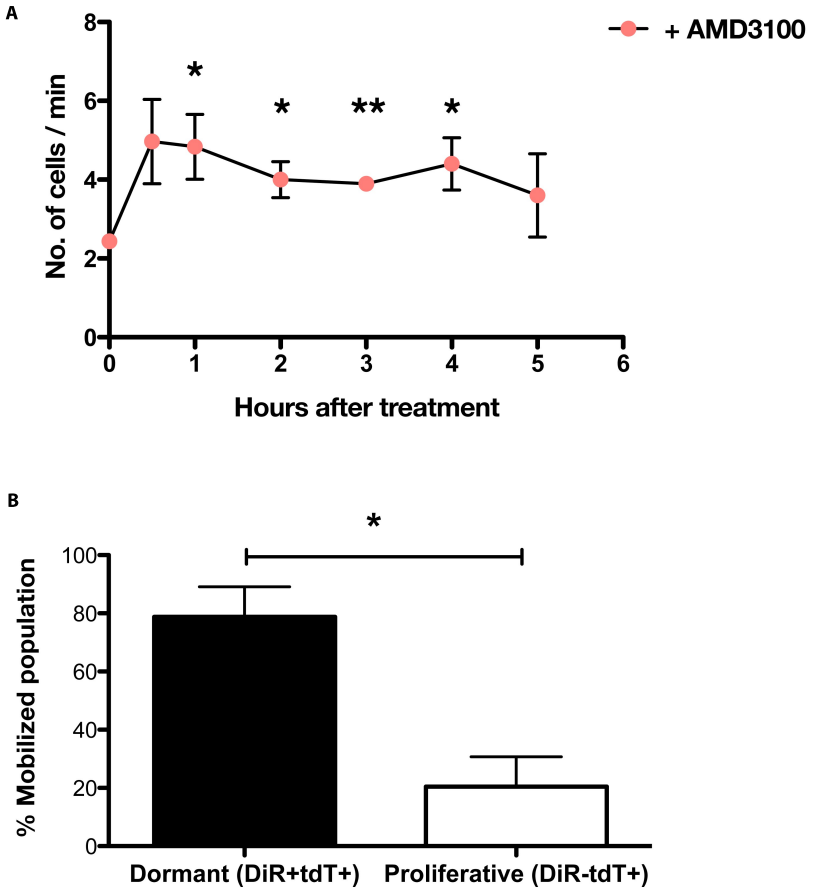

Fig. S22. AMD3100-induced mobilization of dormant BCCs out of the BM and into the circulation. (**A**) 1833 cells were stained with DiD and engrafted in female SCID mice (0.1 x 10^6 cells, I.C. injection). At 20 hours after engraftment, video rate images of the calvarial vasculature were taken. Mice were administered AMD3100 (10 mg/kg, s.c. injection), and videos were recorded at the indicated time points after injection (+0.5 h; +1 h; +2 h; +3 h; +4 h; +5 h). The numbers of cells detected in the vasculature vs. hours after treatment were graphed (*n*=3; **P*=0.0445, +1 h; **P*=0.0297, +2 h; ***P*=0.0017, +3 h; **P*=0.0438, +4; mean +/- SEM; unpaired two-tailed T-test). (**B**) 1833-tdT cells were stained with DiR and engrafted in female SCID mice (0.1 x 10^6 cells, I.C. injection). 6 weeks after engraftment, once disease has been established, mice were imaged before and 2 hours after AMD3100 treatment. A majority of dormant DiR+tdT+ cells were mobilized from the sinusoidal vasculature (78.8 ±10.8; mean +/- SEM, *n*=3, **P*=0.0159).

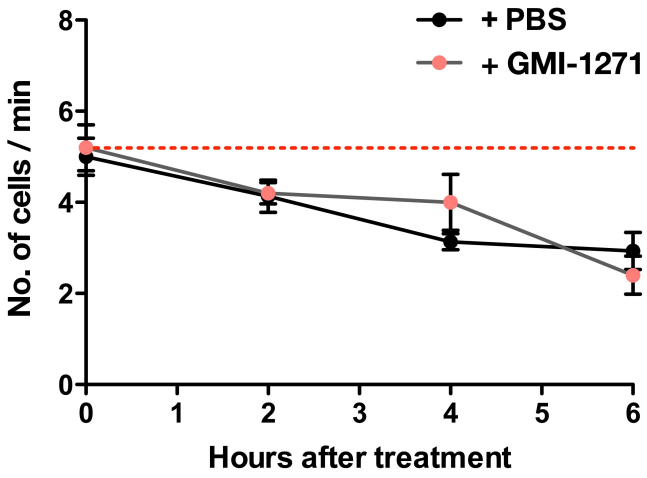

Fig. S23. Lack of effect of GMI-1271 on BCC mobilization from BM. MCF-7 cells were stained with DiD and engrafted in female SCID mice (0.1 x 10^6 cells, I.C. injection). At 20 hours after engraftment, video rate images of the calvarial vasculature were taken. Mice were administered GMI-1271 (40 mg/kg, i.p. injection), and videos were recorded at indicated time points after injection (+2 h; +4 h; +6 h). The numbers of cells detected in the vasculature vs. hours after treatment were graphed (*n*=3; mean +/- SEM).

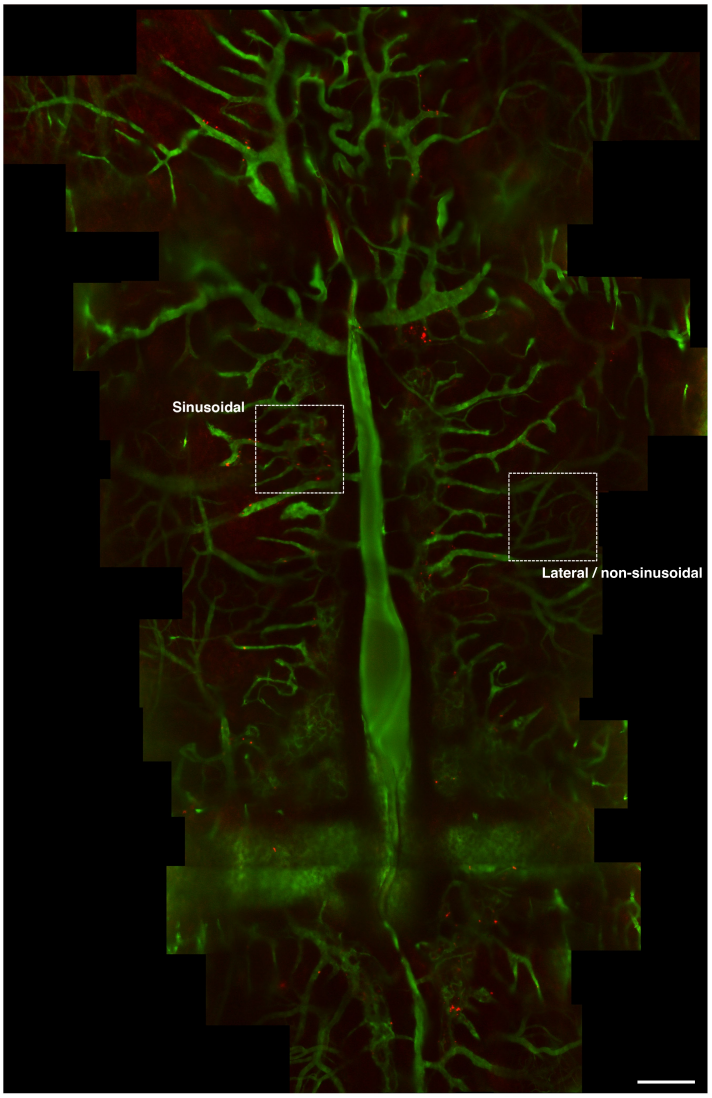

Fig. S24. Montage image of primary human BCC homing to sinusoidal regions of the calvarial BM. Montage image assembled from individual in vivo fluorescent micrographs encompassing the majority of parasagittal sinusoidal vasculature as well as areas of adjacent lateral/non-sinusoidal vasculature of BM. Representative sinusoidal and lateral regions corresponding to the images presented in Fig. 4A are indicated by boxes (red = DiD-labeled primary human BCCs, green = dextran-FITC/vasculature, scale bar = 200 μm).

Supplementary Tables:

Gene Symbol	Name	Aliases	Description
B3GALT1	UDP-Gal:betaGlcNAc beta 1,3-galactosyltransferase, polypeptide 1	beta3Gal-T1	Synthetic enzyme
B3GALT2	UDP-Gal:betaGlcNAc beta 1,3-galactosyltransferase, polypeptide 2	BETA3GALT2, GLCT2, beta3Gal-T2	Synthetic enzyme
B3GALT5	UDP-Gal:betaGlcNAc beta 1,3-galactosyltransferase, polypeptide 5	B3GalT-V, B3GalTx, B3T5, GLCT5, beta-1,3-GalTase 5, beta-3-Gx-T5, beta3Gal-T5	Synthetic enzyme
B3GNT1	beta-1,4-glucuronyltransferase 1	B3GN-T1, B4GAT1, B3GNT6, BETA3GNTI, MDDGA13, iGAT, iGNT	Synthetic enzyme
B3GNT2	UDP-GlcNAc:betaGal beta-1,3-N-acetylglucosaminyltransferase 2	B3GN-T2, B3GNT, B3GNT-2, B3GNT1, BETA3GNT, BGNT2, BGnT-2	Synthetic enzyme
B3GNT3	UDP-GlcNAc:betaGal beta-1,3-N-acetylglucosaminyltransferase 3	B3GAL-T8, B3GN-T3, B3GNT-3, HP10328, TMEM3, beta3Gn-T3	Synthetic enzyme
B4GALT1	UDP-Gal:betaGlcNAc beta 1,4-galactosyltransferase, polypeptide 1	B4GAL-T1, CDG2D, GGTB2, GT1, GTB, beta4Gal-T1	Synthetic enzyme
B4GALT2	UDP-Gal:betaGlcNAc beta 1,4-galactosyltransferase, polypeptide 2	B4Gal-T2, B4Gal-T3, beta4Gal-T2	Synthetic enzyme
B4GALT3	UDP-Gal:betaGlcNAc beta 1,4-galactosyltransferase, polypeptide 3	beta4Gal-T3	Synthetic enzyme

B4GALT4	UDP-Gal:betaGlcNAc beta 1,4-galactosyltransferase, polypeptide 4	B4Gal-T4, beta4Gal-T4	Synthetic enzyme
B4GALT5	UDP-Gal:betaGlcNAc beta 1,4-galactosyltransferase, polypeptide 5	B4Gal-T5, BETA4-GALT-IV, beta4Gal-T5, beta4GalT-V, gt-V	Synthetic enzyme
B4GALT6	UDP-Gal:betaGlcNAc beta 1,4-galactosyltransferase, polypeptide 6	B4Gal-T6, beta4Gal-T6	Synthetic enzyme
CD44	CD44 molecule (Indian blood group)	CDW44, CSPG8, ECMR-III, HCELL, HUTCH-I, IN, LHR, MC56, MDU2, MDU3, MIC4, Pgp1	Ligand
CXCR4	chemokine (C-X-C motif) receptor 4	CD184, D2S201E, FB22, HM89, HSY3RR, LAP-3, LAP3, LCR1, LESTR, NPY3R, NPYR, NPYRL, NPYY3R, WHIM, WHIMS	Receptor
FUT3	fucosyltransferase 3 (galactoside 3(4)-L-fucosyltransferase, Lewis blood group)	CD174, FT3B, FucT-III, LE, Les	Synthetic enzyme
FUT4	fucosyltransferase 4 (alpha (1,3) fucosyltransferase, myeloid-specific)	CD15, ELFT, FCT3A, FUC-TIV, FUTIV, LeX, SSEA-1	Synthetic enzyme
FUT5	fucosyltransferase 5 (alpha (1,3/4) fucosyltransferase)	FUC-TV	Synthetic enzyme
FUT6	fucosyltransferase 6 (alpha (1,3) fucosyltransferase)	FCT3A, FT1A, Fuc-TVI, FucT-VI	Synthetic enzyme
FUT7	fucosyltransferase 7	AI853193, FTVII, Fuc-TVII, FucT-VII	Synthetic enzyme

FUT9	fucosyltransferase 9 (alpha (1,3) fucosyltransferase)	Fuc-TIX	Synthetic enzyme
GLG1	golgi glycoprotein 1	CFR-1, ESL-1, MG-160, MG160	Ligand
LAMP1	lysosomal-associated membrane protein 1	CD107a, LAMPA, LGP120	Ligand
LAMP2	lysosomal-associated membrane protein 2	CD107b, LAMP-2, LAMPB, LGP110	Ligand
LAMP3	lysosomal-associated membrane protein 3	CD208, DC LAMP, DC-LAMP, DCLAMP, LAMP, LAMP-3, TSC403	Ligand
SELL	selectin L	CD62L, LAM1, LECAM1, LEU8, LNHR, LSEL, LYAM1, PLNHR, TQ1	Ligand
SELPLG	selectin P ligand	CD162, CLA, PSGL-1, PSGL1	Ligand
SPN	sialophorin	CD43, GALGP, GPL115, LSN	Ligand
ST3GAL4	ST3 beta-galactoside alpha-2,3-sialyltransferase 4	CGS23, NANTA3, SAT3, SIAT4, SIAT4C, ST3GalIV, STZ	Synthetic enzyme
ST3GAL6	ST3 beta-galactoside alpha-2,3-sialyltransferase 6	SIAT10, ST3GALVI	Synthetic enzyme

Table S1. Gene list. List of 29 candidate genes representing *CXCR4*, *E-selectin* ligands, and enzymes critical for post-translational processing of E-selectin ligands.

Cell Line	Origin	Receptor Status	CXCR4 Expression	Notes
MDA-MB-231	Human	Triple Negative	Low	
1833	Human	Triple Negative	Moderate	Bone-trophic subclone of MDA-MB-231
SUM159	Human	Triple Negative	None	
MCF-7	Human	ER positive	Low	
K1	Human	ER positive	Low	Estrogen-independent subclone of MCF-7
T47D	Human	ER positive	Low	

Table S2. Cell lines. Table of breast cancer cell lines used and listed species of origin, receptor marker status, relative CXCR4 expression profile, and relevant notes applicable to the study.

Supplementary Videos (Uploaded Separately):

Video S1. Circulating BCCs crawling along vascular wall (merge).
Video S2. Circulating BCCs crawling along vascular wall (DiD channel only).

Representative video of MCF-7 cell crawling along vessel wall in the peri-sinusoidal vascular region of the calvarial BM. Fluorescently labeled MCF-7 cells (red) are imaged in the BM microvasculature (green) at video rate after intracardiac engraftment. Both freely circulating and slowly rolling cells are observed. Rolling interactions are a characteristic sign of engagement of vascular E-selectin by circulating cells [green = dextran-FITC; red = DiD; 14 frames per second (FPS)].

Video S3. Circulating BCCs before AMD3100 treatment (merge).
Video S4. Circulating BCCs before AMD3100 treatment (DiD channel only).
Video S5. Circulating BCCs after AMD3100 treatment (merge).
Video S6. Circulating BCCs after AMD3100 treatment (DiD channel only).

Representative videos of AMD3100 mobilization experiment. Fluorescently-labeled 1833 cells (red) were engrafted into female SCID mice (0.1×10^6 cells, I.C injection). At 20 hours after engraftment, video rate images of the calvarial vasculature (central vessel, green) were taken before and 2 hours after administration of the CXCR4 inhibitor AMD3100 (10 mg/kg, s.c. injection). AMD3100 caused mobilization of BCCs out of the BM and a quantifiable increase in DiD+ circulating BCCs [green = dextran-FITC; red = DiD; 14 frames per second (FPS)].